Universality class of triad dynamics on a triangular lattice

Filippo Radicchi,* Daniele Vilone,† and Hildegard Meyer-Ortmanns‡
School of Engineering and Science, International University Bremen, P. O. Box 750561, D-28725 Bremen, Germany
(Received 31 October 2006; revised manuscript received 16 January 2007; published 23 February 2007)

We consider triad dynamics as it was recently considered by Antal *et al.* [Phys. Rev. E **72**, 036121 (2005)] as an approach to social balance. Here we generalize the topology from all-to-all to the regular one of a two-dimensional triangular lattice. The driving force in this dynamics is the reduction of frustrated triads in order to reach a balanced state. The dynamics is parametrized by a so-called propensity parameter p that determines the tendency of negative links to become positive. As a function of p we find a phase transition between different kinds of absorbing states. The phases differ by the existence of an infinitely connected (percolated) cluster of negative links that forms whenever $p \leqslant p_c$. Moreover, for $p \leqslant p_c$, the time to reach the absorbing state grows powerlike with the system size L, while it increases logarithmically with L for $p > p_c$. From a finite-size scaling analysis we numerically determine the static critical exponents β and $\nu_\perp$ together with γ, τ, σ, and the dynamical critical exponents $\nu_\parallel$ and δ. The exponents satisfy the hyperscaling relations. We also determine the fractal dimension d_f that satisfies a hyperscaling relation as well. The transition of triad dynamics between different absorbing states belongs to a universality class with different critical exponents. We generalize the triad dynamics to four-cycle dynamics on a square lattice. In this case, again there is a transition between different absorbing states, going along with the formation of an infinite cluster of negative links, but the usual scaling and hyperscaling relations are violated.

DOI: 10.1103/PhysRevE.75.021118 PACS number(s): 05.40.−a, 64.60.Ak, 89.75.Fb

I. INTRODUCTION

Recently Antal *et al.* [1] proposed a so-called triad dynamics to model the approach to social balance [2–4]. An essential ingredient in the algorithm is the reduction of frustration in the following sense. We assign a value of +1 or −1 to a link (or bond) in the all-to-all topology if it connects two individuals who are friends or enemies, respectively. We call the sign ±1 of a link its spin. If the product of links along the boundary of a triad is negative, the triad is called frustrated (or imbalanced), otherwise it is called balanced (or unfrustrated). The state of the network is called balanced if all triads are balanced. The algorithm depends on a parameter $p \in [0,1]$, called the propensity parameter. It determines the tendency of the system to reduce frustration via flipping a negative link to a positive one. For an all-to-all topology Antal *et al.* predict a transition from an imbalanced nonabsorbing stationary state for $p < 1/2$ to a balanced absorbing state for $p \geqslant 1/2$. Here the dynamics is motivated by social applications so that the notion of frustration from physics goes along with frustration in the psychological sense. The mathematical criterion for checking the status of frustration is the same.

In a recent paper [5] we generalized the triad dynamics in two aspects. The first generalization refers to a k-cycle dynamics which contains the triad dynamics for $k=3$. Here it turned out that the main difference comes from the difference of whether k is even or odd, since the phase structure is symmetric about $p=1/2$ for k even. Even in the infinite-volume limit there are only absorbing states, apart from the transition point at $p=1/2$. The second generalization concerned the network topology from all-to-all connections to a diluted network. We studied the phase structure as a function of the propensity p and the dilution. As it turned out, the diluted k-cycle dynamics can be mapped on a certain satisfiability problem in computer science, the so-called k-XOR-SAT problem [6], and socially balanced states in one problem correspond to all logical constraints satisfied in the k-XOR-SAT problem. In both models we have phases of imbalanced nonabsorbing states in the infinite-volume limit, separated by a phase transition from phases of balanced or absorbing states. In a finite volume one only observes balanced states, but as a remnant of the infinite-volume phase structure, the time to reach the absorbing states differs in a characteristic way.

In this paper we study triad dynamics on a two-dimensional triangular lattice and four-cycle dynamics (called tetrad dynamics) on a square lattice. From the interpretation as an approach to social balance, triad or tetrad dynamics on a regular topology are not more realistic than on an all-to-all topology. Still, triad dynamics shows interesting features in terms of a percolation transition if we compare snapshots of frozen states for different values of p. Also for tetrad dynamics we observe a transition between different absorbing states, but the description in terms of a percolation transition fails. As we shall see, due to the restrictive topology, imbalanced triads and tetrads allow only two elementary processes: either they diffuse or they annihilate each other. As a result, the system always approaches a balanced absorbing state; nevertheless we observe a transition as a function of the propensity parameter p, this time between different absorbing states. The difference is characterized by the presence or absence of an infinite cluster of connected unfriendly (negative) links and for triad dynamics by the time to reach these frozen states. The parameter p should not be confused with the occupation probability of a single bond with a posi-

*Electronic address: f.radicchi@iu-bremen.de
†Electronic address: d.vilone@iu-bremen.de
‡Electronic address: h.ortmanns@iu-bremen.de

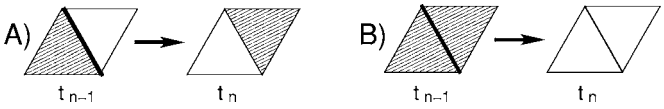

FIG. 1. Local dynamics of one update event. The imbalanced triads are represented as filled triangles, while the balanced ones as empty triangles. The shared link is represented as bold; this is the link involved in the update event. (a) When the update event flips the link shared by one imbalanced and one balanced triad we have diffusion. (b) When the update event flips the link shared by two imbalanced triads we have annihilation.

tive sign as it is usually used in connection with bond percolation. Therefore, here for $p \leqslant p_c$ we observe an infinite cluster of negative links, while such a cluster is absent for $p > p_c$. For triad dynamics the time to reach the frozen state grows logarithmically with the system size for $p > p_c$ and as a power of the size for $p \leqslant p_c$. In contrast, for tetrad dynamics it grows as a power of the system size only at the transition point, while it grows logarithmically above and below p_c. For triad dynamics we numerically determine the critical exponents from a finite-size scaling analysis of the frozen patterns. We analyze the probability P_∞ for a link to belong to the infinite cluster that serves as an order parameter as well as the order parameter susceptibility and the distribution of clusters of finite size s. The static critical exponents β, $\nu_\perp$, γ, σ, and τ satisfy the usual hyperscaling relations as well as the fractal dimension d_f and the dynamical critical exponents $\nu_\parallel$ and δ. The critical exponents turn out to be new and completely different from those of standard percolation in two dimensions [7,8].

The outline of the paper is the following. In Sec. II we define the triad dynamics on a triangular lattice. In Sec. III we analyze the finite-volume dependence of the frozen states as a function of the propensity parameter p and present the results for the static critical exponents as well as for the fractal dimension. Moreover, we analyze the finite-time dependence of the geometrical properties of the evolving states as a function of p and report the values of the dynamical critical exponents. Section IV deals with tetrad dynamics on a square lattice for which the hyperscaling relations are violated. In Sec. V we summarize the conclusions.

II. TRIAD DYNAMICS

Our dynamical system is defined on an undirected graph (network) composed of nodes and links. Each link (i,j) between the nodes i and j takes spin values $\sigma_{(i,j)}=-1$ or $\sigma_{(i,j)}=+1$ if the nodes i and j are "enemies" or "friends," respectively. A triad $[\triangle]$ (i,j,k) is characterized by the values assigned to its three links (i,j), (j,k), and (k,i). We have four types of triads, depending on the number of negative links they contain in their boundary: Δ_0, Δ_1, Δ_2, and Δ_3, where the subscript stands for the number of negative (or "unfriendly") links. We use the standard notion of *social balance* as proposed in [2,3] and apply this notion to triads. The sign of a triad is defined as the product of the spins assigned to the links of the triad. A triad is considered as "balanced" or "unfrustrated" if its sign is positive, otherwise it is called

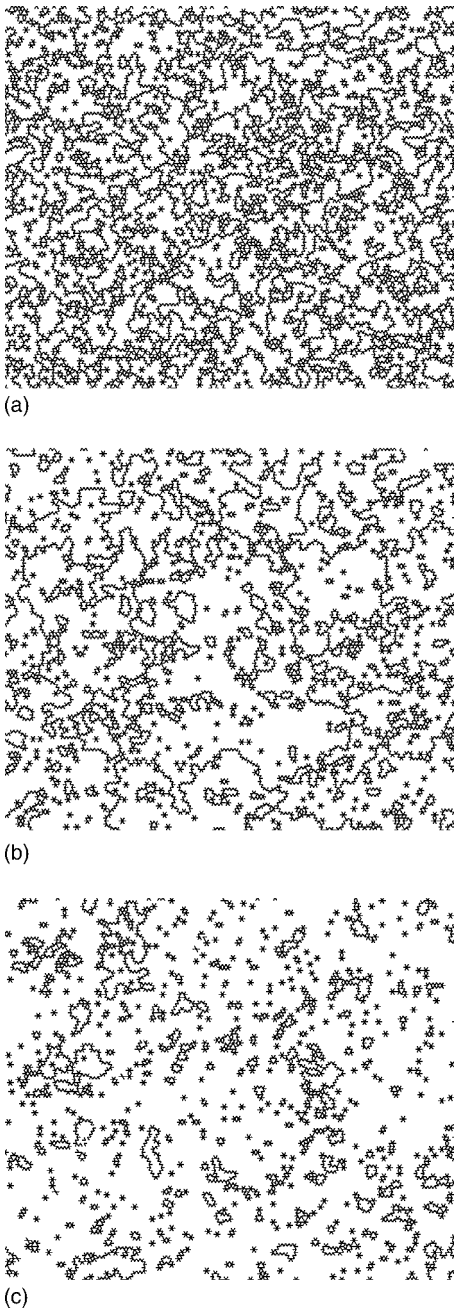

FIG. 2. Typical frozen configurations for a triangular lattice with periodic boundary conditions, with linear size $L=129$ and for different values of p: (a) $p=0.44$, (b) $p=p_c=0.4625$, (c) $p=0.48$. In the plots only negative links are shown.

"imbalanced" or "frustrated." The triads Δ_0 (all friends) and Δ_2 (two friends have the same enemy) are balanced, while the triads Δ_1 and Δ_3 are imbalanced. The network itself is called balanced if and only if all triads belonging to the network are balanced.

As in [1,5] we perform a local unconstrained dynamics in order to reduce the frustration of the network. As it turns out, the local algorithm always drives the network to a fully balanced state without frustrated triads, but the time it needs for reaching the frozen state depends on the choice of parameters. At each update event one triad is selected at random. If

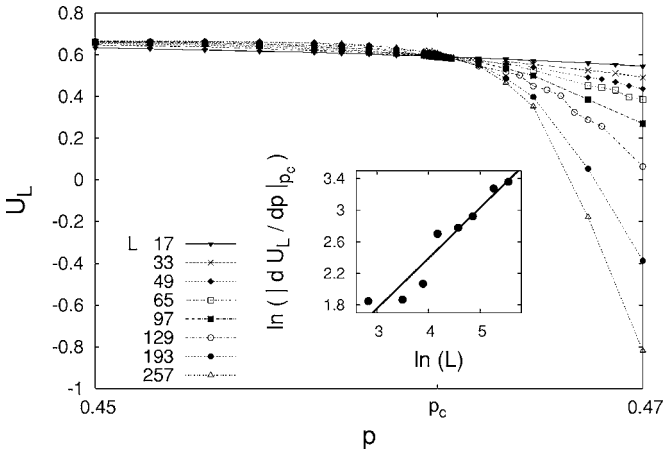

FIG. 3. Binder cumulant U_L as a function of the propensity parameter p. The main plot shows U_L in the vicinity of the critical point. The numerical results for different linear lattice sizes L have a common intersection at $p_c \simeq 0.4625$. The inset shows the ln-ln plot of $|dU_L/dp|_{p_c}$. From the relation $|dU_L/dp|_{p_c} \sim L^{1/\nu_\perp}$ we find $1/\nu_\perp = 0.64(7)$ (solid line).

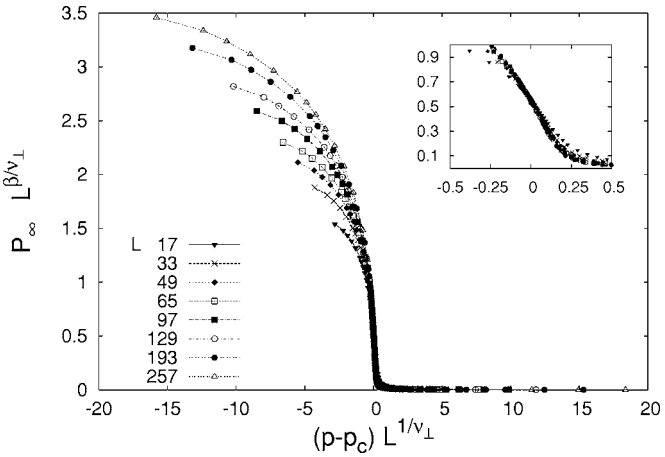

FIG. 5. Same data as in Fig. 4, but now the abscissa is rescaled according to $(p-p_c)L^{1/\nu_\perp}$ with $1/\nu_\perp = 0.64$. The inset shows a zoom around zero. The numerical simulations are the same as in Fig. 3.

the selected triad is balanced (type Δ_0 or Δ_2) nothing happens. If the selected triad is imbalanced (type Δ_1 or Δ_3) it is updated into a balanced one by flipping one of its link. In particular a triad Δ_1 is changed with probability p into a triad Δ_0 (flipping the only negative link of the triad Δ_1), and it is changed with probability $1-p$ into a triad Δ_2 (choosing at random one of the two positive links belonging to the triad Δ_1 and inverting the spin to a negative value). A triad Δ_3 is changed into a triad Δ_2 with probability 1, choosing at random one of its three negative links and reversing its spin to a positive sign. We summarize the updating rules of the local algorithm in the following scheme:

$$\Delta_0 \underset{p}{\leftarrow} \Delta_1 \xrightarrow[1-p]{} \Delta_2 \underset{1}{\leftarrow} \Delta_3. \tag{1}$$

One time unit has passed when the number of single update events equals the total number of links M of the network.

We study the triad dynamics on two-dimensional triangular lattices with periodic boundary conditions. We characterize a triangular lattice using its linear size L. The total number of sites in the lattice is $N=L(L-1)$. The term $L-1$ results from the periodic boundary conditions. The total number of links of the lattice is $M=3N$, while the total number of triads is $N_\Delta=2N$. In particular each link is shared only by two nearest-neighbor triads, so that the triad dynamics cannot increase the total number of imbalanced triads: a single update changes one selected imbalanced triad into a balanced one, while it modifies the other triad, sharing the same updated link, either from balanced to imbalanced [Fig. 1(a)] or from imbalanced to balanced [Fig. 1(b)]. The former we call

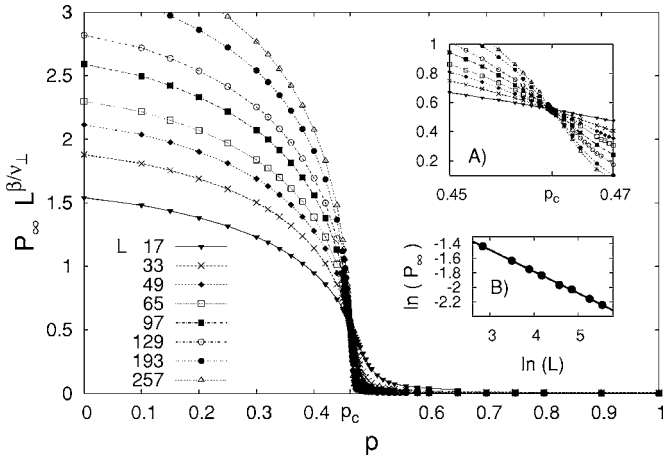

FIG. 4. Probability P_∞ that a bond belongs to the largest cluster as a function of p and for different linear sizes of the lattice. We perform a finite-size scaling for determining the critical point $p_c = 0.4625(5)$ [see the zoom around the critical point in the inset (a)] with the critical exponents $\beta/\nu_\perp = 0.297(3)$ (solid line) as is shown in the inset (b), where P_∞ at the critical point is plotted as a function of the linear size of the lattice L. The numerical simulations are the same as in Fig. 3.

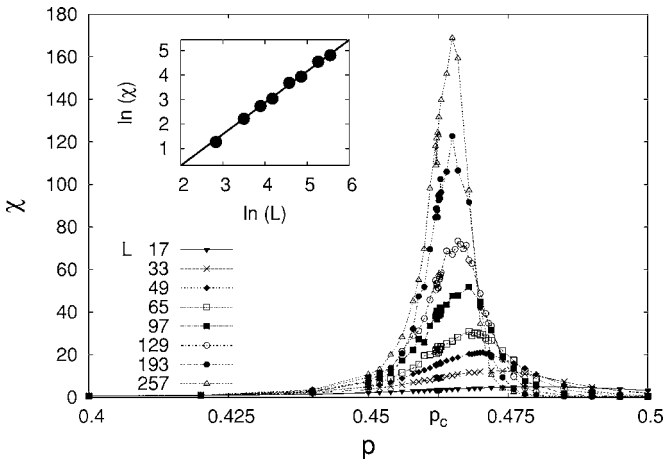

FIG. 6. Susceptibility χ of P_∞ as a function of p. In the main plot we zoom the region around the critical point p_c, while in the inset we plot χ at the critical point as a function of L leading to $\gamma/\nu_\perp = 1.28(3)$ (solid line). The numerical simulations are the same as in Fig. 3.

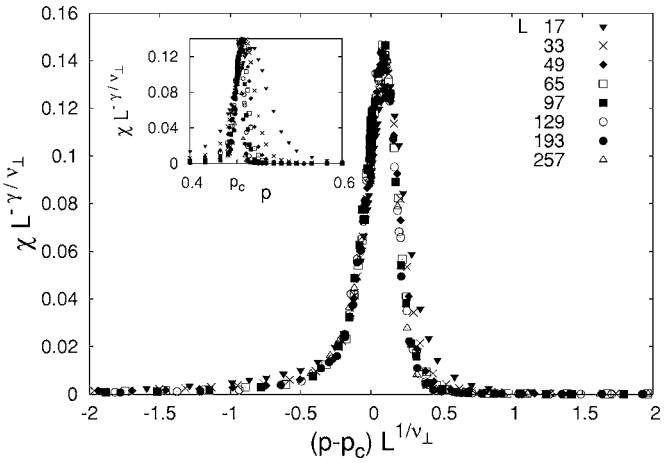

FIG. 7. Finite-size scaling for the susceptibility χ. The data are the same as in Fig. 6. In the inset we zoom the function $\chi L^{-\gamma/\nu_\perp}$ around the critical point p_c, while in the main plot we rescale the abscissa as $(p-p_c)L^{1/\nu_\perp}$. The critical exponents are chosen as $\gamma/\nu_\perp=1.28$ and $1/\nu_\perp=0.64$.

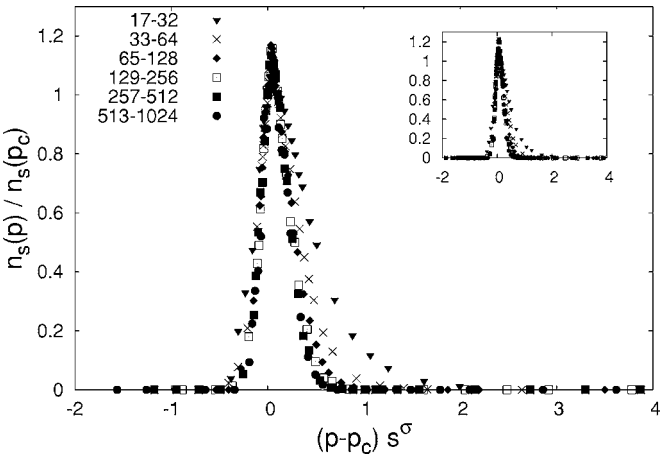

FIG. 9. Numerical test of the validity of Eq. (7). We plot the ratio $n_s(p)/n_s(p_c)$, where n_s is the distribution of the cluster size, as a function of the rescaled quantity $(p-p_c)s^\sigma$ with σ chosen as 0.41 from Eq. (13) knowing β and γ. The main plot refers to $L=257$, the inset to $L=129$.

diffusion, because the imbalanced triad diffuses, the latter annihilation between two imbalanced triads.

Obviously, for a finite-size system we always observe a frozen configuration as the stationary state (see Fig. 2), independently of the initial configuration. From now on we focus on these frozen configurations and study their geometrical properties by using the standard tools of percolation theory [7]. It should be noticed, however, that the dynamical parameter p of the triad dynamics is very different from the occupation probability as it is defined in percolation theory, where it is also called p.

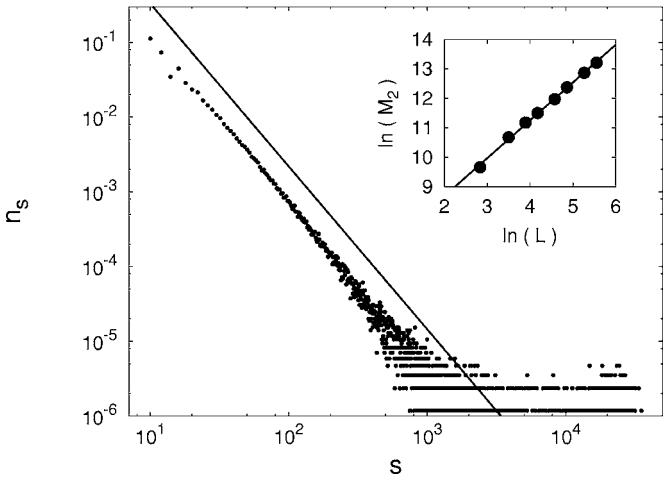

FIG. 8. Distribution of the cluster size $n_s(p_c)$ at the critical point p_c and for $L=257$ (main graph). The distribution is extracted from 10^3 frozen configurations. As expected this distribution follows a power law $n_s \sim s^{-\tau}$; the solid line plotted here corresponds to $\tau=2.19$. The inset shows the second moment of the distribution of the cluster size M_2 at the critical point as a function of the linear size of the lattice. M_2 increases as a power of the linear size L of the lattice with exponent $\gamma/\nu_\perp=1.28(2)$ (solid line).

III. NUMERICAL SIMULATIONS TO DETERMINE THE CRITICAL THRESHOLD AND THE CRITICAL EXPONENTS

In order to study the geometry of the frozen configurations, we consider the distribution of negative links on the lattice. In particular we numerically compute the probability that a negative link belongs to an infinite cluster $P_\infty = M_\infty^- / M$, as the ratio of the number of links belonging to the largest cluster of connected negative links M_∞^- to the total number of links M.

A. Critical propensity parameter p_c

Let us first determine the critical point p_c. Binder's cumulant [9], defined as the fourth-order reduced cumulant of the probability distribution

$$U_L = 1 - \frac{\langle P_\infty^4 \rangle}{3\langle P_\infty^2 \rangle^2}, \tag{2}$$

allows us to determine the critical point p_c without tuning any parameter. In Eq. (2) $\langle \cdot \rangle$ stands for the average over all realizations of the distribution. It is known that the Binder cumulant should satisfy the scaling relation [9]

$$U_L = \tilde{U}[(p-p_c)L^{1/\nu_\perp}], \tag{3}$$

with $\tilde{U}(\cdot)$ a universal function. From Fig. 3 it is obvious that the Binder cumulants for different linear sizes of the lattice L have a common intersection at $p=0.4625(5)$, so that we use $p_c=0.4625$ as the critical propensity parameter in the following analysis. The numerical results of Fig. 3 are extracted from numerical simulations for $L=17$, 33, 49, 65, 97, 129, 193, and 257. The averages are taken over several frozen configurations as they are reached as absorbing states of the triad dynamics, starting from initial conditions where each link is randomly assigned a value of +1 or −1 with the same probability 1/2. The number of realizations is 10^4 for values of L up to 65 and 10^3 for larger values of L.

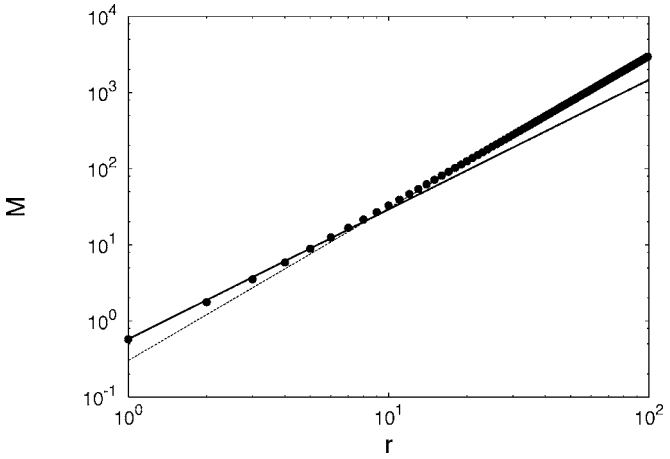

FIG. 10. Mass of negative links M inside a triangular box with r links per side. The mass is measured on a triangular lattice with $L=257$ and periodic boundary conditions. Each point is given by the average over 10^3 frozen configurations, while the number of boxes considered for each r is 10^2. The numerical results fit a power law with $d_f=1.703$ (solid line) and $d=2$ (dotted line).

B. Critical exponent $\nu_\perp$

In order to extract the value of the critical exponent $\nu_\perp$ that characterizes the divergence of the correlation length $\xi_\perp$ in the vicinity of the critical point, we consider the absolute value of the first derivative of the Binder cumulant calculated at p_c, $|dU_L/dp|_{p_c}$. We expect from Eq. (3) to have $|dU_L/dp|_{p_c} \sim L^{1/\nu_\perp}$. This relation is actually satisfied for $1/\nu_\perp=0.64(7)$ as it is seen in the inset of Fig. 3, from which $\nu_\perp=1.6(2)$. For the numerical estimate of the derivative of U_L we use $|dU_L/dp|_{p_c}=|\Sigma_{q=1}^{Q} q a_{L,q} p_c^{q-1}|$ where the coefficients $a_{L,q}$ are obtained by interpolating the cumulant U_L with a polynomial $U_L=\Sigma_{q=0}^{Q} a_{L,q} p^q$. Here we choose $Q=5$ and restrict the interpolation to the interval [0.46,0.465].

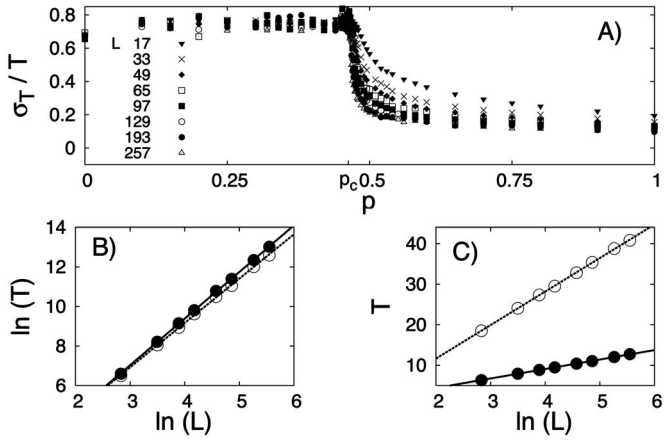

FIG. 11. Average time T needed for reaching a frozen configuration. The data sets are the same as in Fig. 3. In (a) we plot the standard variance σ_T over the average value T as a function of p and for different values of L. The peaks of this ratio are all around the critical point p_c. In (b) we show a ln−ln plot of T as a function of the linear size of the lattice L at the critical point p_c (full circles) and at $p=1/3$ (open circles). It implies that $T\sim L^z$ for $p\leqslant p_c$. We have $z=2.36(1)$ (solid line) at p_c, while $z=2.24(2)$ (dotted line) at $p=1/3$. In (c) the plot of T versus the logarithm of L for $p=1$ (full circles) and 3/4 (open circles) shows that $T\sim \ln(L)$ for $p>p_c$. The numerical simulations are the same as in Fig. 3.

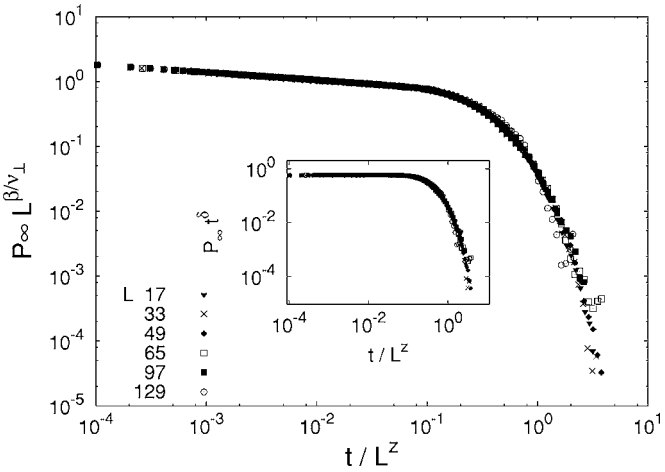

FIG. 12. Finite-size scaling of the time-dependent behavior of the percolation probability $P_\infty(t)$. The values of the critical exponents used here are $\beta/\nu_\perp=0.297$, $z=2.36$, and $\delta=0.126$. The numerical results are obtained by averaging over 10^4 realizations for $L=17$ and 33, 10^3 realizations for $L=49$ and 65, and 10^2 realizations for $L=97$ and 129.

C. Critical exponent β

According to percolation theory, the probability P_∞ satisfies the following finite-size scaling relation:

$$P_\infty = L^{-\beta/\nu_\perp} \tilde{P}[(p-p_c)L^{1/\nu_\perp}], \tag{4}$$

where p_c is the critical value of the propensity parameter p for which the phase transition occurs. (In the infinite-volume limit we have $P_\infty=1$ for $p\leqslant p_c$, while $P_\infty=0$ for $p>p_c$.) $\tilde{P}(\cdot)$ is a universal function. A plot of $P_\infty L^{\beta/\nu_\perp}$ as a function of p and for different values of L is shown in Fig. 4. For a value of $\beta/\nu_\perp=0.297(3)$ [see inset (b)] all curves have an intersection in $p_c=0.4625(5)$ as is more obvious from the inset (a). Using for $\nu_\perp$ the value calculated so far, we obtain $\beta=0.46(5)$.

If we rescale the abscissa as $(p-p_c)L^{1/\nu_\perp}$ with $p_c=0.4625$ and $1/\nu_\perp=0.64$, all curves for different values of L collapse into one (see Fig. 5). This is true especially close to zero as the inset of Fig. 5 clearly shows.

D. Critical exponent γ

Moreover, in Fig. 6 we plot the susceptibility

$$\chi = M[\langle P_\infty^2\rangle - \langle P_\infty\rangle^2], \tag{5}$$

in which we only show a zoom around $p=p_c$, while in the inset we plot the value of χ, at the critical point, as a function of the linear size of the lattice L. From the inset we find $\gamma/\nu_\perp=1.28(3)$, because $\chi\sim L^{\gamma/\nu_\perp}$ at p_c; therefore $\gamma=2.0(3)$. The susceptibility should satisfy the finite-size scaling relation

$$\chi = L^{\gamma/\nu_\perp} \tilde{\chi}[(p - p_c)L^{1/\nu_\perp}], \tag{6}$$

where again $\tilde{\chi}(\cdot)$ is a universal function. This relation is perfectly satisfied (cf. Fig. 7).

E. Critical exponents τ and σ

Furthermore, we consider the probability distribution of having n_s clusters with s negative links. n_s is given by the ratio of the number of clusters of size s to the total number of clusters. As it is known from percolation theory, n_s should satisfy

$$n_s = s^{-\tau} \tilde{n}[(p - p_c)s^\sigma], \tag{7}$$

where τ and σ are critical exponents and $\tilde{n}(\cdot)$ is a universal function. We can determine the critical exponent τ (also called the Fisher exponent) by plotting the distribution of the cluster sizes s at the critical point p_c. This distribution is calculated in Fig. 8 for $L=257$. The distribution fits with a power law $s^{-\tau}$, here plotted as solid line with $\tau=2.19$. We checked that the same exponent fits also for smaller values of L.

In Fig. 9 we numerically determine the critical exponent σ. The figure shows the plot of the ratio $n_s(p)/n_s(p_c)$. Using the rescaled variable $(p-p_c)s^\sigma$ as abscissa, all the curves corresponding to different values of the cluster size s ($2^4 < s \leq 2^5$, $2^5 < s \leq 2^6$, $2^6 < s \leq 2^7$, etc.) collapse to a single function for $\sigma=0.41$, as expected (see, e.g., [7]).

F. Check of the critical exponent γ

From the cluster distribution it is possible to verify the value of the critical exponent γ that was calculated before. It is known that the second moment of the distribution of the cluster size

$$M_2 = \sum_s s^2 n_s \tag{8}$$

should scale according to $M_2 \sim L^{\gamma/\nu_\perp}$ at the critical point p_c. The numerical value found for the ratio $\gamma/\nu_\perp = 1.28(2)$ is consistent with the former one obtained via the susceptibility (see the inset of Fig. 8).

G. Fractal dimension d_f

The percolating cluster can be further characterized in terms of a fractal dimension d_f. The fractal dimension d_f is easily computed using a box counting method [8]. We count how many negative links $M(r)$ belong to a triangular box with r links per side. The measurement is performed for $L=257$ at the critical point p_c. We analyze 10^3 frozen configurations, for each of them we consider 10^2 different boxes. The mass $M(r)$ per box is plotted in Fig. 10. As expected we observe the crossover phenomenon

$$M(r) = \begin{cases} r^{d_f} & \text{if } r \ll \xi_\perp, \\ r^d & \text{if } r \gg \xi_\perp, \end{cases} \tag{9}$$

where $d=2$ in this case. The numerical results fit with a power law with $d_f=1.703$ and $d=2$, respectively.

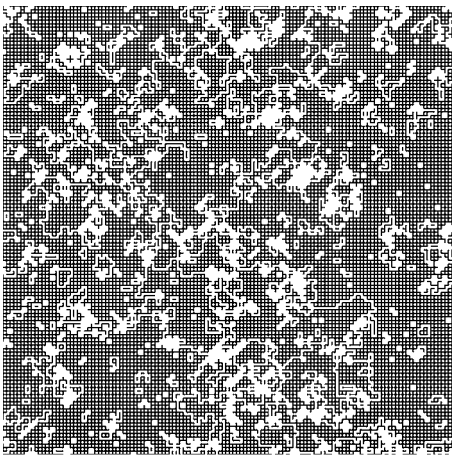

(a)

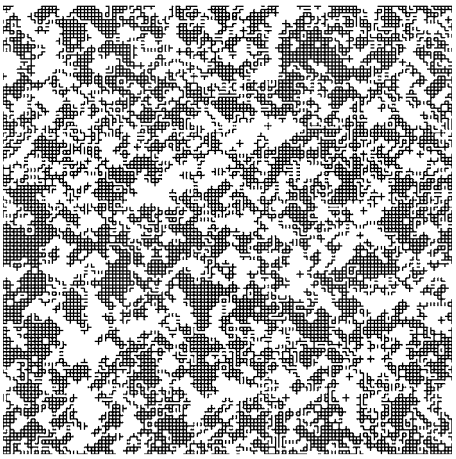

(b)

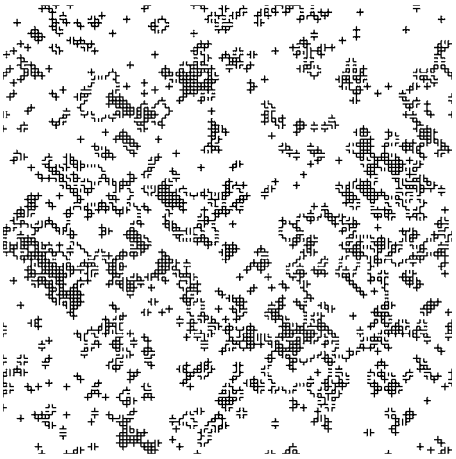

(c)

FIG. 13. Typical frozen configurations for a square lattice with periodic boundary conditions, with linear size $L=128$ and for different values of p: (a) $p=0.48$, (b) $p=p_c=0.5$, (c) $p=0.52$. In these plots are shown only the negative links.

H. Time to reach the frozen states

So far we have characterized the geometrical properties of the final absorbing configuration. As a next step we focus on the dynamical features and determine the time the system

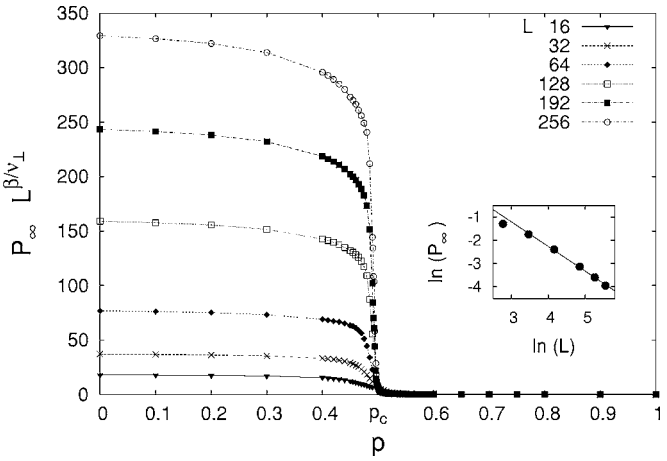

FIG. 14. Probability P_∞ that a link belongs to the largest cluster as a function of p and for different linear sizes of the lattice. The ratio of critical exponents $\beta/\nu_\perp=1.05(2)$ at the critical point $p_c=0.5$ is shown in the inset.

needs to reach the final frozen configurations. In Fig. 11(a) we plot the ratio of the variance σ_T and its average value T as a function of p. It is interesting to notice that σ_T/T has a maximum around p_c. Below the critical point p_c, the relaxation time T is governed by a power-law relation in the linear size of the lattice L: $T\sim L^z$. Our numerical analysis reveals $z=2.36(1)$ at p_c and $z=2.24(1)$ at $p=1/3$ [see Fig. 11(b)]. Furthermore, above the critical point p_c, T grows logarithmically with L: $T\sim\ln(L)$ [see Fig. 11(c), where we show the L dependence of T for $p=3/4$ and for $p=1$]. The different size dependence of the time the system needs to reach a frozen configuration in both phases can be understood in qualitative terms. For $p>p_c$ there is a lower probability for having negative links. The stable configurations forming out of these links are mainly local objects like star-like configurations which do not percolate through the lattice [see Fig. 1(c)]. Therefore the time to reach such a state characterized by local objects depends weakly on the system size, that is logarithmically. For $p\leqslant p_c$ there is a high probability of having negative links. However, here large loops that finally percolate through the lattice make up the stable configurations [see Figs. 1(a) and 1(b)]. So the time to reach this configuration is more sensitive to the system size: it grows as a power of the size.

I. Dynamical critical exponents $\nu_\parallel$ and δ

The existence of the dynamical critical exponent z suggests the possibility to analyze the percolation transition of our model from a dynamical point of view. Therefore we performed other numerical simulations with the aim of determining some dynamical critical exponents. We followed a procedure similar to the one usually applied for other time-dependent critical phenomena [10]. Starting from a fully occupied lattice [i.e., all the links of the triangular lattice are set to be negative so that $P_\infty(t=0)=1$], we observe how P_∞ evolves in time. According to finite-size scaling analysis we should expect, at the critical point p_c, a behavior of the type

TABLE I. Critical threshold and critical exponents, numerically determined for triad dynamics on two-dimensional triangular lattices. The critical exponents of triad dynamics on triangular lattices are compared with those of standard percolation in two dimensions (which does not have any dynamical exponents).

	Triad dynamics	Percolation in two dimensions[7]
p_c	0.4625(5)	
β	0.46(5)	$5/36\simeq0.138$
γ	2.0(3)	$43/18\simeq2.388$
$\nu_\perp$	1.6(2)	$4/3\simeq1.333$
σ	0.41(6)	$36/91\simeq0.396$
τ	2.19(1)	$187/91\simeq2.055$
d_f	1.703(3)	$91/48\simeq1.895$
$\nu_\parallel$	3.8(5)	None
δ	0.126(1)	None

$$P_\infty(t)\sim L^{-\beta/\nu_\perp}f(t/L^z), \tag{10}$$

where $f(\cdot)$ is a suitable universal function. We numerically test the validity of this relation. In Fig. 12 we plot $P_\infty(t)L^{\beta/\nu_\perp}$ versus t/L^z, for $p=p_c$ and various lattice sizes L. The values of $\beta/\nu_\perp$ and z calculated above are consistent with Eq. (10), since all curves for different values of L collapse into a single curve. In analogy with other time-dependent critical phenomena [10,11], we may look at z as the ratio between the critical exponent $\nu_\parallel$ of the typical time-correlation length $\xi_\parallel$ of the percolation cluster and $\nu_\perp$ as the typical spatial correlation length $\xi_\perp$. This means $z=\nu_\parallel/\nu_\perp$, therefore knowing $\nu_\perp$ and z, we estimate $\nu_\parallel$ to be 3.8(5).

Moreover we determine the critical exponent δ of the time decay of P_∞ at the critical p_c: $P_\infty(t)\sim t^{-\delta}$. [$P_\infty(t)$ is expected to decay to zero at p_c, because there the ratio of links belonging to the infinite cluster over all links is still vanishing in the infinite volume. Choosing a different initial value of P_∞ at time $t=0$ leads to the same powerlike long-time behavior in time, so $P_\infty(0)=1$ is chosen for convenience.] Therefore, by means of the same simulations as used before it is possible to test the validity of the scaling relation

$$P_\infty(t)\sim t^{-\delta}g(t/L^z), \tag{11}$$

where $g(\cdot)$ is a proper universal function. We show the result of this numerical test in the inset of Fig. 12, where we impose $\delta=0.126$. The actual value of δ used in this plot is obtained from the known values of β and $\nu_\parallel$ and the hyperscaling relation of Eq. (15) that connect the three critical exponents β, $\nu_\parallel$ and δ. The numerical results reported in both plots of Fig. 12 are obtained by averaging over a large number of realizations (10^4 for $L=17$ and 33, 10^3 for $L=49$ and 65, 10^2 for $L=97$ and 129).

J. Universality class of triad dynamics in two dimensions

We list the critical exponents for the phase transition between different absorbing states in Table I. The critical exponents satisfy the known hyperscaling relations. For ex-

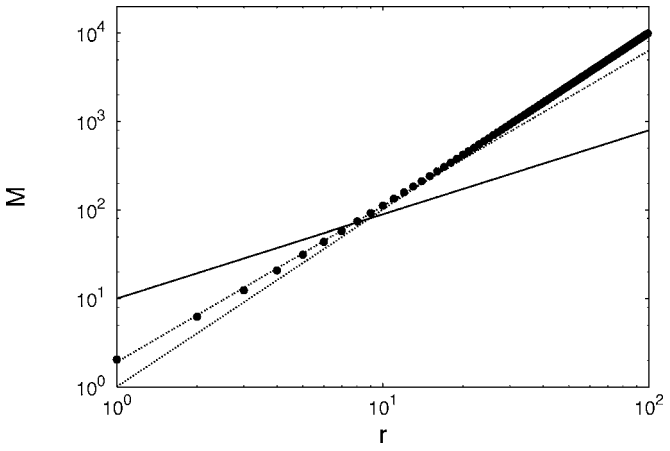

FIG. 15. Mass of negative links M inside a square box with r links per side. This measure is used on a square lattice with $L=256$ and periodic boundary conditions. Each point is given by the average over 10^3 frozen configurations, while the number of boxes considered at each r is 10^3. The solid line has the slope 0.95, a value that is expected by the former measure of $\beta/\nu_\perp$. Actually it is not consistent with the direct fit of the data from which we find $d_f=1.76(2)$ (dashed line). The dotted line has slope $d=2$.

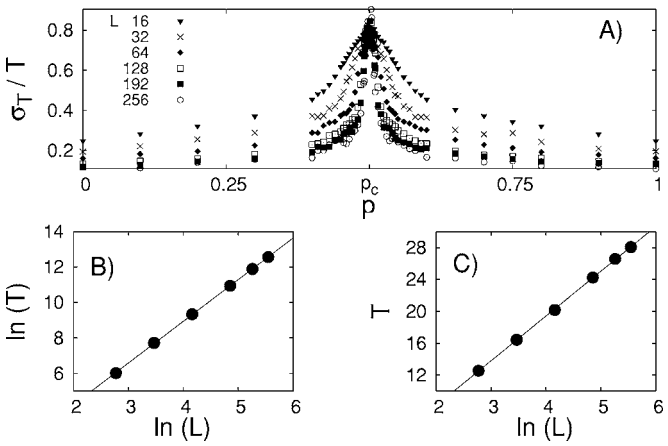

FIG. 16. Average time T needed for reaching a frozen configuration. The simulations are the same as in Fig. 14. In (a) we plot the standard variance σ_T over the average value T as a function of p and for different values of L. The peaks of this ratio are all in the vicinity of the critical point p_c. In (b) we show a ln-ln plot of T as a function of the linear size of the lattice L at the critical point leading to $T\sim L^z$ with $z=2.35(1)$. In (c) the plot of T versus the logarithm of L for $p=1$ shows that $T\sim\ln(L)$.

ample, it is known from percolation theory that the critical exponents β, γ, τ, and σ are related by

$$\tau=\frac{1}{2}\left(5-\frac{\gamma-\beta}{\gamma+\beta}\right) \tag{12}$$

and

$$\sigma=\frac{1}{\gamma+\beta}. \tag{13}$$

Calculating τ and σ from the former equations, using the numerically obtained values of β and γ, we find $\tau=2.19(1)$ and $\sigma=0.41(6)$. Both values are consistent with Figs. 8 and 9.

The fractal dimension is related to the ratio $\beta/\nu_\perp$ by the hyperscaling relation

$$d_f=d-\frac{\beta}{\nu_\perp}. \tag{14}$$

From this relation we find $d_f=1.703(3)$ in agreement with Fig. 10.

The exponent of the time-decay of the percolation probability $P_\infty(t)\sim t^{-\delta}$ at the critical point is related to the critical exponents β and $\nu_\parallel$ by the hyperscaling relation [10]

$$\delta=\frac{\beta}{\nu_\parallel}. \tag{15}$$

From this relation we calculate $\delta=0.126(1)$ in agreement with Fig. 12.

The errors of p_c and of the critical exponents as indicated in Table I arise as follows. The critical point p_c is directly estimated from Fig. 3, verified in Fig. 4, and supported by Fig. 10. The only source of error here is given by the step size used for varying the propensity parameter p. Of course this step size is related to the parameters of the simulations. It can be decreased by increasing the system size and the total number of simulations.

The critical exponents $\beta/\nu_\perp$ of Fig. 4(b), $1/\nu_\perp$ of Fig. 3, $\gamma/\nu_\perp$ of Figs. 7 and 8, and z of Fig. 11 have errors due to the linear fit in a double-logarithmic plane. In principle one should also account for the propagation of the error entering the value of the critical point $p_c=0.4625(5)$, which we have neglected here.

In order to check the validity of the hyperscaling relations we evaluate the corrections to all derived quantities (τ, σ, d_f, $\nu_\parallel$, and δ) by using the standard formula for error propagation. The hyperscaling relations are then said to be satisfied if they hold within these error bars.

To our knowledge the critical exponents calculated so far are new [7,8,11]. Therefore, the percolation transition between different absorbing states of triad dynamics on two-dimensional lattices can be described by standard percolation theory, but the transition seems to belong to a new universality class.

IV. TETRAD DYNAMICS

The notion of social balance can be extended to any geometric figure with k links (in graph theory denoted as k-cycles) [3,5]. As it turned out in [5] for an all-to-all topology and a diluted topology, generalizing the triad dynamics to a k-cycle dynamics leads to qualitative differences in the phase structure of which the main differences are due to k being even rather than being larger than three. In this section we therefore focus on the case of $k=4$ and call the four-cycles tetrads defined on square lattices. According to the number of negative links belonging to a particular tetrad, we distinguish five types of tetrads: $\square_0$, $\square_1$, $\square_2$, $\square_3$, $\square_4$. The updating rules of the unconstrained dynamics for triads of (1)

are naturally extended to tetrads in the following way:

$$\square_0 \underset{p}{\leftarrow} \square_1 \xrightarrow[1-p]{} \square_2 \underset{p}{\leftarrow} \square_3 \xrightarrow[1-p]{} \square_4. \tag{16}$$

The local tetrad dynamics is then applied to square lattices with periodic boundary conditions. L denotes the linear size of the lattice, i.e. the number of sites per row or per column. The total number of sites of the lattice is $N=L^2$, the total number of links $M=2N$, and the total number of tetrads $N_{\square}=N$.

Similarly to the case of triad dynamics on two-dimensional triangular lattices, at a first glance there seems to be a percolation transition also in case of tetrad dynamics. The critical point p_c should be equal to $p_c=0.5$ due to the symmetry of the system (16) under the simultaneous transformation $\sigma_i \rightarrow -\sigma_i \forall i$ and $p \rightarrow 1-p$ (see Fig. 13).

However, differently from the triad dynamics, no scaling relations hold in the vicinity of the transition at which again an infinite cluster of negative links forms. The hyperscaling relations are violated. For example, the relation (14) does not hold because one can measure $\beta/\nu_{\perp}=1.05(2)$ (Fig. 14) and expect to have $d_f=0.95(2)$, while it is directly seen from Fig. 15 that $d_f=1.76(2)$.

Tetrad dynamics resembles triad dynamics. Either each unstable tetrad diffuses, or two unstable tetrads annihilate if they meet. Finite-size systems always reach a frozen configuration within a finite time, so we can measure this time T. As we can see from Fig. 16(a), we find a symmetric behavior around the critical point p_c. At the critical point T scales according to $T \sim L^z$ with $z=2.35(1)$ [see Fig. 16(b)], this value is actually consistent with the one found for the triad dynamics. Away from the critical point $T \sim \ln(L)$ [see Fig. 16(c)].

V. SUMMARY AND CONCLUSIONS

The driving force in triad dynamics is the reduction of the number of frustrated triads. A state of zero frustration is called a state of social balance. Imposed on a triangular lattice, frustrated triads can diffuse or annihilate each other. Depending on the value of the propensity parameter p the final absorbing state can be characterized by the absence ($p > p_c$) or presence ($p \leqslant p_c$) of an infinite cluster of negative links. The time to reach the frozen configurations scales with the system size in a way that further characterizes the phases: it scales logarithmically for $p > p_c$ and in a powerlike way for $p \leqslant p_c$. The static critical exponents $\nu_{\perp}$, β, γ, τ, and σ as well as the fractal dimension d_f and the dynamical critical exponents $\nu_{\parallel}$ and δ satisfy hyperscaling relations within the error bars. The values of these exponents seem to characterize a new universality class. The essential difference that we observe for tetrad dynamics on a square lattice is the symmetry between the absorbing states in the different phases. Again, an infinite cluster of negative links forms for $p \leqslant p_c$, but the time to reach the frozen configurations shows the same dependence on the system size in both phases, with the only exception at the transition point. The percolation picture breaks down in the sense that no scaling and therefore no hyperscaling relations are satisfied.

[1] T. Antal, P. L. Krapivsky, and S. Redner, Phys. Rev. E **72**, 036121 (2005).

[2] F. Heider, Psychol. Today **51**, 358 (1944); Sankhya **21**, 107 (1946); *The Psychology of Interpersonal Relations* (John Wiley & Sons, New York, 1958); S. Wasserman and K. Faust, *Social Network Analysis: Methods and Applications* (Cambridge University Press, New York, 1994).

[3] D. Cartwright and F. Harary, Psychol. Rev. **63**, 277 (1956); F. Harary, R. Z. Norman, and D. Cartwright, *Structural Models: An Introduction to the Theory of Directed Graphs* (John Wiley & Sons, New York, 1965).

[4] F. Harary, Mich. Math. J. **2**, 143 (1953-54); F. S. Roberts, Electronic Notes in Discrete Mathematics (ENDM) **2**, 94 (1999); N. P. Hummon and P. Doreian, J. Ship Prod. **25**, 17 (2003).

[5] F. Radicchi, D. Vilone, S. Yoon, and H. Meyer-Ortmanns, Phys. Rev. E **75**, 026106 (2007).

[6] M. R. Garey and D. S. Johnson, *Computer and Intractability: A Guide to the Theory of NP-Completeness* (Freeman, San Francisco, 1979).

[7] D. Stauffer, *Introduction to Percolation Theory* (Taylor and Francis, London, 1985).

[8] A. Bunde and S. Havlin, *Fractals and Disordered Systems* (Springer, New York, 1996); D. ben-Avraham and S. Havlin, *Diffusion and Reactions in Fractals and Disordered Systems* (Cambridge University Press, Cambridge, U.K., 2000).

[9] K. Binder, Z. Phys. B: Condens. Matter **43**, 119 (1981); K. Binder and D. W. Heerman, *Monte Carlo Simulation in Statistical Physics* (Springer-Verlag, Berlin, 1997).

[10] H. Hinrichsen, Adv. Phys. **49**, 7 (2000).

[11] G. Ódor, Rev. Mod. Phys. **76**, 663 (2004).